Rapid #: -20911409

CROSS REF ID: **560579**

LENDER: **NJR (Rutgers University) :: Main Library**

BORROWER: **TEU (Temple University) :: Main Library**

TYPE:	Article CC:CCL
JOURNAL TITLE:	Advances in engineering software
USER JOURNAL TITLE:	Advances in Engineering Software
ARTICLE TITLE:	Constructive algorithms of vascular network modeling for training of minimally invasive catheterization procedure
ARTICLE AUTHOR:	Cai, Yiyu
VOLUME:	34
ISSUE:	7
MONTH:	
YEAR:	2003
PAGES:	439-450
ISSN:	0965-9978
OCLC #:	

Processed by RapidX: 6/20/2023 5:43:45 AM

ELSEVIER

Advances in Engineering Software 34 (2003) 439–450

ADVANCES IN ENGINEERING SOFTWARE

www.elsevier.com/locate/advengsoft

Constructive algorithms of vascular network modeling for training of minimally invasive catheterization procedure

Yiyu Cai[a,*], Xiuzi Ye[b,c], Cheekong Chui[d,e], James H. Anderson[f]

[a]*School of Mechanical and Production Engineering, Nanyang Technological University, 50 Nanyang Avenue, Singapore 639798, Singapore*
[b]*Zhejiang University, People's Republic of China*
[c]*Solidworks Corporation, Concord, Boston, MA 01742, USA*
[d]*Graduate School of Frontier Science, University of Tokyo, Tokyo, Japan*
[e]*Institute of Bioengineering and Nanotechnology, Singapore*
[f]*School of Medicine, Johns Hopkins University, Baltimore, MD, USA*

Received 19 September 2002; revised 15 January 2003; accepted 20 February 2003

Abstract

In this paper, three-dimensional modeling of vascular networks is described. We propose a constructive approach to generating vascular segments and bifurcations using sweeping and blending operations. This allows smooth connection of individual branching segments at the vascular bifurcations. A tangential continuity or visual smooth (e.g. GC^1) representation of the vascular network is derived to formulate constructive algorithms for vascular modeling. The vascular modeling technique developed is applied in our medical simulation system for the training and pretreatment planning of minimally invasive vascular surgery using catheterization procedure.

Keywords: Three-dimensional modeling; Vascular network; Geometric continuity; Bifurcation

1. Introduction

Three-dimensional (3D) vascular network modeling is one of the fundamental tasks in vascular medical imaging, reconstruction and visualization. Chen and Carroll studied the problem of 3D reconstruction of coronary arterial tree for angiographic visualization [1]. Optimization techniques for modeling of 3D vascular trees were discussed by several researchers [1–3]. Accurate vascular network model is increasingly recognized as the crucial component for many applications including bio-mechanics or haemo-dynamics studies [4–6]. With the 3D vascular networks, real-time and realistic simulation of vascular catheterizations can be developed [7]; and vascular devices and implants can be optimally designed and verified in a computational environment [8]. In clinical applications, measurements of vascular lesions are critical in diagnosing vascular diseases such as abdominal aortic aneurysms and carotid artery stenosis, and subsequently, for pretreatment planning [9–14].

Not like mechanical parts, vascular networks demonstrate very complicated structures and thus efficient techniques for modeling of vascular system are highly wanted. Besides, adequate representation scheme for such tree-like vascular shapes is also crucial for high quality vascular model development. We propose a constructive approach to modelling the complicated vascular networks that offer several advantages over the traditional solutions: (1) vascular networks are reconstructed in a high fidelity manner from the vascular images thus allowing natural integration of vascular modeling process with the patient-specific medical imaging; (2) surface-based 3D vascular format is selected thus avoiding data-crunching volumetric representation for sparse vascular networks; (3) surface representation also offers better control of modeling accuracy especially with our constructive solution for the highly complicated vascular joint modeling; (4) uniform modeling strategy for segmental and bifurcation structures provides more efficient solutions for hierarchical representation and realistic visualization of the vascular networks,

* Corresponding author. Tel.: +65-679-05777; fax: +65-679-11859.
E-mail address: myycai@ntu.edu.sg (Y. Cai).

0965-9978/03/$ - see front matter © 2003 Elsevier Science Ltd. All rights reserved.
doi:10.1016/S0965-9978(03)00035-8

and make their further applications such as real-time medical simulation and Level of Detail (LOD) feasible.

In the following, we first review the state-of-the-art for vascular tree reconstruction. A constructive approach to modeling visual smooth vascular networks is then presented. The geometric continuity representations of vascular segments and bifurcations are developed. Vascular segments are modeled using sweeping operation while vascular bifurcations are modeled using sweeping-based blending operation. Based on the GC^1 conditions for boundaries and cross-boundary derivatives, constructive algorithms for segmental sweeping and bifurcation blending are designed. The applications of this surface-centered vascular modeling techniques are also demonstrated before we conclude the paper.

2. Literature review

Vascular modeling research is primarily conducted in two main tracks. Volume-originated methods start with vascular modeling from volumetric vascular data. The volumetric data are typically Computerized Tomography or Magnetic Resonance Imaging digital images. Lorensen et al. pioneered the 'Marching Cubes' algorithm to extract iso-surfaces from image sets [15]. Typically, a large numbers (easily millions level) of triangles will be generated with such algorithms. This is computationally expensive in terms of both space and time. Mesh simplification and the LODs techniques have been developed to compress the triangle numbers with reasonable compromises of rendering performance and quality [16,17]. Volume rendering methods employ algorithms like ray casting that shoots rays through a volume object from each pixel in the image. It tri-linearly interpolates samples along each ray and provides complex shading calculations and color assignments at the sample points, which are then accumulated into the final pixel colors [18]. Real-time volume rendering with hardware texture mapping (e.g. SGI) for UNIX platform or with board card (e.g. Mitsubishi VolumePro) for PC platform are commercially available. Several improved algorithms using iso-surfacing or volume rendering techniques have been developed to visualize branching vascular systems [19–21].

Projection-originated methods reconstruct 3D vascular geometry from two or more images [22–24]. In Computer Vision [25], 3D reconstruction from biplane projections represents an ill-defined mathematical problem and additional information is needed to obtain a valid solution [26,27]. Often, thinning methods of 'active-contour', 'medial axis transformation', 'simulated annealing', etc. are employed to determine the vascular information in the projection planes [28–32]. The advantage of projective reconstruction is its capability to handle tiny tube-like systems such as neurovascular, neural and lymphatic vessels that could be easily lost with conventional iso-surfacing techniques.

Piece-by-piece cylinder or generalized cylinder representations of the vasculature are widely used in vascular modeling [33,34]. Polygonal tessellation, e.g. triangulation, is also commonly applied to model 3D tube-like shapes [44,45]. Van Leeuwen et al. [35] defined potential function along the vessel network. Implicit surface methods for skeletal reconstructions of branching shapes have been developed [36]. Accurate modeling of 3D vascular networks very much relies on a good representation of vascular segments and bifurcations. Ideally, the vascular model should be visually smooth and the detail of graphical vascular displays should be adaptive depending on the application requirement.

3. Formulation

3.1. Tube sweeping

Surface sweeping is a powerful tool for creating tube-like shape. The sweeping operation requires a smooth trajectory and cross-sectional shapes. To form a tube-like surface, a closed cross-sectional contour must be used. Surface sweeping operation, however, applies to either open or closed cross-sectional curve. We use a cubic Bézier curve to represent the central trajectory or path. Let $\gamma(t)$ be any of GC^1 paths, a local coordinate system $(T(t), N(t), B(t))$ can be defined along the curve (Fig. 1). This triplet $(T(t), N(t), B(t))$, known as Frenet frame, is the tangent, normal and bi-normal defined along the trajectory. Assume $r(t)$ is a contour function, not necessarily circular, defined in the cross-sectional plane perpendicular to the curve at a given point along the trajectory. The sweeping surface can be represented as [37,38]:

$$\Gamma(t, \theta) = \gamma(t) + r(t)(\cos\theta N(t) + \sin\theta B(t)) \quad (1)$$

where θ is the cross-sectional angle and $t \in [0, 1]$ is a parameter defined along the curve. It is not difficult to model the thickened tubes if inner and outer cross-sectional curves are provided.

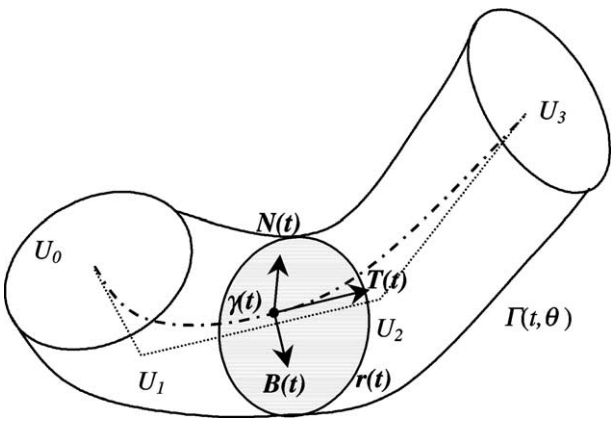

Fig. 1. Surface sweeping.

3.2. GC^1 condition for three-sided hole

Three surfaces $\Gamma_i(\mu_i, \theta)$, $(i = 1, 2, 3)$ are connected with tangential continuity at their corners to form a triangle hole (Fig. 3). Let $C_i(\mu_i)$ $(i = 1, 2, 3)$ be three boundary curves.

We now take a look on the tangent conditions at the corners and boundaries of the filling triangle. Obviously, the tangents of $C_1(\mu_1)$ and $C_2(\mu_2)$ at Θ_1 are the same. We denote them as T_1 (Fig. 2). Similarly, we have T_2 at Θ_2, and T_3 at Θ_3. Let the tangents of the boundary curves $\Gamma_1(0, \theta)$ and $\Gamma_3(1, \theta)$ incident to Θ_1 be $T_{1,1}$ and $T_{1,3}$, respectively. In general, the tangent of the boundary curves of $\Gamma_i(0, \theta)$ and $\Gamma_{i-1}(1, \theta)$ incident to Θ_i are denoted by $T_{i,i}$ and $T_{i,(i-1)}$. Similarly, the second order derivatives of the boundary curves of $\Gamma_i(0, \theta)$ and $\Gamma_{i-1}(1, \theta)$ incident to Θ_i are denoted by $N_{i,i}$ and $N_{i,(i-1)}$. Note that mode operation by three is used whenever the subscript index is larger than three or less than one. The vector-valued cross-boundary derivatives of Φ along $C_i(\mu_i)$ are denoted by $D\Phi_i(\mu_i)$, $(i = 1, 2, 3)$ while the vector-valued cross-boundary derivatives of $\Gamma_i(\mu_i, \theta)$ along $C_i(\mu_i)$ are denoted by $D\Gamma_i(\mu_i)$, $(i = 1, 2, 3)$.

Tangent at corners. The condition for the surfaces to be tangent at Θ_i is that the tangent plane at Θ_i is unique. That is to say, T_i, $T_{i,(i-1)}$ and $T_{i,i}$ are coplanar. In other words, there exist real numbers α_i and β_i such that

$$T_{i,(i-1)} = \alpha_i T_{i,i} + \beta_i T_i \tag{2}$$

Tangent along hole boundaries. Along $C_i(\mu_i)$, at any point, the condition for surfaces Γ_i and Φ to be tangent is that the following three vectors $D\Phi_i(\mu_i)$, $D\Gamma_i(\mu_i)$, and $C_i'(\mu_i)$ are coplanar. This means that there exist functions $p_i(\mu_i)$ and $q_i(\mu_i)$ such that

$$D\Phi_i(\mu_i) = p_i(\mu_i)\cdot D\Gamma_i(\mu_i) + q_i(\mu_i)\cdot C_i'(\mu_i) \tag{3}$$

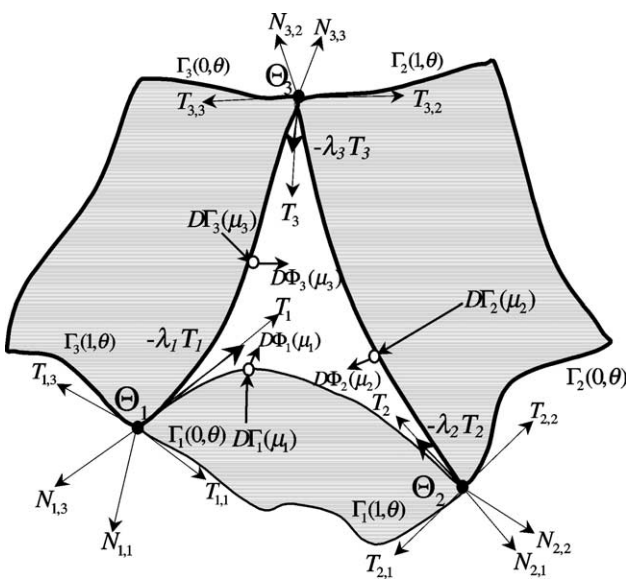

Fig. 2. Tangential continuity along three-sided hole boundaries.

At vertices Θ_i and Θ_{i+1} since

$$\begin{aligned} &D\Phi_i(0) = \lambda_i T_i, \\ &D\Phi_i(1) = T_{i+1} D\Gamma_i(0) = T_{i,i}, \qquad D\Gamma_i(1) = T_{i+1,i} \end{aligned} \tag{4}$$

We have from Eqs. (3) and (4)

$$p_i(0) = p_i(1) = 0; \qquad q_i(0) = \lambda_i; \qquad q_i(1) = -\lambda_{i+1}^{-1} \tag{5}$$

Twist compatibility. Mathematically, twist compatibility is the property of a surface indicating sequence independence for the differentiation of the surface twists, namely, the second order mixed partial derivatives. At any interior point along $C_i(\mu_i)$, the twist compatibility is automatically ensured [39]. At the corner vertices Θ_i, however, the twist compatibility may not be the case unless the following condition holds:

$$\frac{\mathrm{d}}{\mathrm{d}\mu_{i-1}}(D\Phi_{i-1}(\mu_{i-1}))\Big|_{\mu_{i-1}=1} = \frac{\mathrm{d}}{\mathrm{d}\mu_i}(D\Phi_i(\mu_i))\Big|_{\mu_i=0} \tag{6}$$

Differentiating Eq. (3) about μ_i and from Eqs. (2), (4) and (6), we have

$$\begin{aligned} &\lambda_i C_i''(0) + p_i'(0) T_{i,i} + q_i'(0) T_i \\ &\quad = -\lambda_i^{-1} C_{i-1}''(1) + \alpha_i p_{i-1}'(1) T_{i,i} - \lambda_i q_{i-1}'(1) T_i \end{aligned} \tag{7}$$

or

$$\begin{aligned} C_i''(0) = &-\lambda_i^{-2} C_{i-1}''(1) + \lambda_i^{-1}(\alpha_i p_{i-1}'(1) - p_i'(0)) T_{i,i} \\ &- (q_{i-1}'(1) + \lambda_i^{-1} q_i'(0)) T_i \end{aligned} \tag{8}$$

We now determine the scalar functions $p_i(\mu_i)$ and $q_i(\mu_i)$. Satisfying Eq. (5) with $p_i'(1) = 2\xi_i, (\xi_i > 0)$, $(i = 1, 2, 3)$, $p_i(\mu_i)$ and $q_i(\mu_i)$ can be constructed in the following quadratic and linear forms, respectively:

$$\begin{aligned} p_i(\mu_i) &= p_i(0)(1 - \mu_i)^2 + 2\xi_i(1 - \mu_i)\mu_i + p_i(1)\mu_i^2 \\ &= 2\xi_i(1 - \mu_i)\mu_i \end{aligned} \tag{9}$$

$$q_i(\mu_i) = q_i(0)(1 - \mu_i) + q_i(1)\mu_i = \lambda_i(1 - \mu_i) - \lambda_{i+1}^{-1}\mu_i$$

Here $\xi_i > 0$, $(i = 1, 2, 3)$ serves as shape fullness parameters. The larger the parameter ξ_i, the greater the influence of $D\Gamma_i(\mu_i)$ on $D\Phi_i(\mu_i)$, and thus, the greater the magnitude of vector $D\Phi_i(\mu_i)$. As a result, the fullness of the hole filling patches increases.

Unique existence of the tangent plane at corners. The tangent plane of a surface $S(u, v)$ at a non-singular point P is determined by S_u and S_v at P. However, if S_u and S_v are parallel at P, P will be a singular point of $S(u, v)$ and the tangent plane of $S(u, v)$ at P may not exist. If it exists, it must involve the second order partial derivative vectors of surface S, i.e. (S_{uu}, S_{uv}, S_{vv}). This can be seen from the Taylor expansion of S at the neighborhood of P. It is also clear from the Taylor expansion that if $(S_u, S_v, S_{uu}, S_{uv}, S_{vv})$ spans one and only one plane at P, the existence and uniqueness of the tangent plane of $S(u, v)$ at P is guaranteed. This is because, the difference vector between every point Q (in

the neighborhood of P) and P, up to the second order Taylor expansion, lies on this plane.

Now, considering the tangent planes Π_i of $\Phi_i(u,v)$ at Θ_i $(i=1,2,3)$. At Θ_i, the semi-tubular surfaces incident to Θ_i are tangent to the plane spanned by $(T_i, T_{i,i})$. The tangent plane of $\Phi_i(u,v)$ at singularity Θ_i, if there is any, is determined according to Taylor expansion by T_i, $C_i''(0)$, $C_{i-1}''(1)$ and the twist vector. Eq. (8) indicates that $C_{i-1}''(1)$ is a linear combination of T_i, $T_{i,i}$ and $C_i''(0)$. Therefore, the tangent plane of $\Phi_i(u,v)$ at Θ_i, if there is any, is determined by T_i, $T_{i,i}$ and $C_i''(0)$.

In summary, if $C_i''(0)$ lies on the plane spanned by $(T_i, T_{i,i})$ at Θ_i of the semi-tubular surfaces incident to Θ_i, the tangent plane of $\Phi_i(u,v)$ at Θ_i uniquely exists and all the surfaces incident to Θ_i have a common tangent plane Π_i at Θ_i. We can modify $C_i(\mu_i)$ so that $C_i''(0)$ lies on the plane Π_i.

4. Algorithms

4.1. Piecewise construction of GC^1 segmental curve

Fig. 3 shows the construction of a piecewise vascular path. A smooth curve in the cubic Bézier form (dark) is generated based on the four given nodes V_{i-1}, V_i, V_{i+1}, V_{i+2}. This piece of curve is formed with a tagential continuity at V_i and V_{i+1}. Parameters ε_i and δ_i serve as factors controlling the curve shape and intermediate vertice V_i^1 and V_i^2 can be obtained. The unit vector v_{i+1} is normalized with a direction chosen as $(V_{i+2} - V_i)$. At the curve ends, the unit vectors should be calculated separately. Given node sequence $\{V_i, i=0,\ldots,n\}$, the GC^1 vessel curve is constructed in a piecewise manner as follows.

(i) At each node V_i, a unit vector can be determined $v_i = (V_{i+1} - V_{i-1})/\|V_{i+1} - V_{i-1}\|$.
(ii) With parameters ε_i and δ_i, a control polygon with vertice V_i^0, V_i^1, V_i^2 and V_i^3 is formed.
(iii) Cubic Bézier curve can be generated from the control polygon.
(iv) Repeat the above steps and, piecewise cubic Bézier curves can be formed from the given nodes.

4.2. Construction of GC^1 vessel bifurcation curves

Fig. 4 is an illustration showing the construction of three cubic Bézier curves as bifurcation trajectories. These three trajectories are generated from a given triangle of vertices W_1, W_2 and W_3. W_0 is an internal vertex in the triangle that has three branches characterized with vectors W_0W_1, W_0W_2 and W_0W_3. Let vector v_i $(i=1,2,3)$ be the normalized branch vector. Three control polygons $W_1U_1U_2W_2$, $W_2U_2U_3W_3$ and $W_3U_3U_1W_1$ can be formed within the triangle. The parameter U_i $(i=1,2,3)$ gives a freedom of shape control. The vectors v_i $(i=1,2,3)$ can be used as starting tangent vectors for the neighboring piece to construct segmental surfaces. Note that the three central trajectories have tangential contacts at their common ends. The procedure to construct the bifurcation trajectories can be described in the following:

(i) Three branch vectors are calculated by $v_i = W_0W_i/\|W_0W_i\|$, $i=1,2,3$.
(ii) Three intermediate vertice U_i are used to form three cubic control polygons $W_1U_1U_2W_2$, $W_2U_2U_3W_3$ and $W_3U_3U_1W_1$.
(iii) Three cubic Bézier curves are generated based on three control polygons.

4.3. Segmental tubular sweeping

To model blood vessels, cross-sectional contours and trajectories are required. The trajectories constructed above can serve as the central sweeping paths in a piecewise cubic Bézier form. The cross-sectional contour, however, should also be represented in cubic Bézier form. To do so,

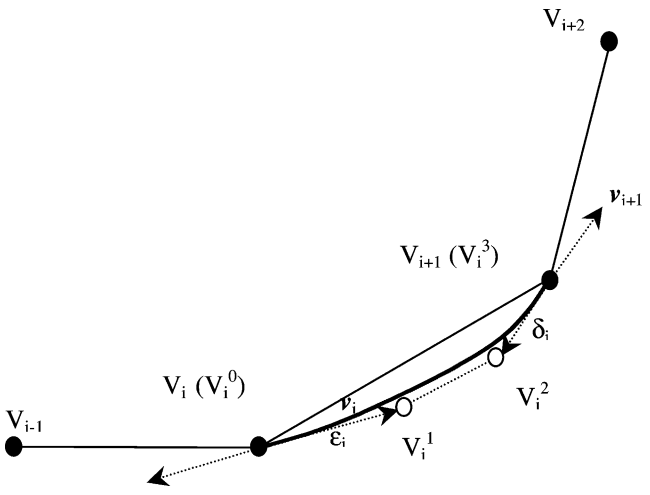

Fig. 3. Piecewise construction of cubic G^1 Bézier curve.

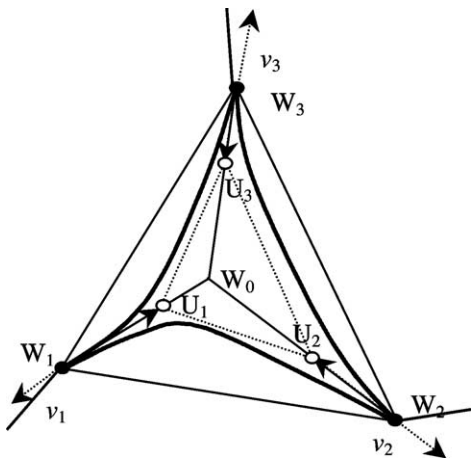

Fig. 4. Construction of bifurcation trajectories.

the method in Ref. [40] is used to describe two semi-circles in cubic Bézier form. Here the commonly accepted assumption of blood vessels having round shapes is accepted. Therefore, the surface sweeping technique described earlier can be applied. We need two bi-cubic Bézier patches to form a closed vessel segment. The cross-sectional radii are required to generate the Bézier patches. If inner radius and outer radius are provided with each node, one can generate a thickened vascular segment. To verify and avoid self-intersection of the swept surface, the singularity check approach proposed in Ref. [41] can be applied. The segmental tubular sweeping algorithm has the following steps:

(i) piecewise construction of a central path with given nodes using the algorithm described in Section 4.1;
(ii) construction of two half circles in cubic Bézier form with given radii at the ends of each trajectory piece;
(iii) piecewise construction of two bi-cubic Bézier patches with each given trajectory and cross-sectional half circle.

4.4. Bifurcation semi-tubular sweeping

A joint is a place where individual branching information joins together. Based on this concept, we model the bifurcation in such a way that every two branching segments are blended using sweeping operations. In addition, all three branching segments are also blended for the final bifurcation formation. With three trajectories available, surface sweeping can be performed to form the joint surface following the algorithm for segmental tubular sweeping. Obviously, only half of the tubular surface can be used in order to avoid self-intersection (Fig. 5). This, however, leads to an absence of two triangular patches (front and back) with the joint. The bifurcation modeling is, therefore, converted to the problem of the three-sided hole filling. In other words, the complete solution of joint modeling requires a seamless sewing of two triangular patches. This is a typical n-sided hole filling problem. To generate G^1 smooth bifurcation, however, additional efforts for surface modification are desired. Below is the algorithm for bifurcation tubular sweeping:

(a) piecewise construction of three bifurcation trajectories with the given bifurcation nodes using the algorithm described in Section 4.2;
(b) construction of two half circles in cubic Bézier form with given radii at each of three branches;
(c) piecewise construction of three bi-cubic Bézier patches with each bifurcation trajectory and cross-sectional half circle.

4.5. Hole filling using Gregory–Zhou approach

Due to symmetry, only front filling ($\theta = 0$) will be addressed here (the back filling deals with $\theta = \pi$). To fill the triangular hole with given neighboring surfaces, we use an analytic approach described in Ref. [42]. The boundary curves $C_i(\mu_i)$ $(i = 1, 2, 3)$ are split into two $C_{i,0}(\mu_i)$ and $C_{i,1}(\mu_i)$ at $\mu_i = 1/2$ so that the triangle filling problem is converted to three rectangle fillings with given boundary conditions inherited from their split neighbors (Fig. 6). With this approach, it is guaranteed that a cross-boundary tangential continuity can be achieved along their star-lines, namely, the common boundaries among the three rectangular patches. See Ref. [42] for more information about the algorithm.

So far, the bifurcation model is generated using all bi-cubic Bézier forms. However, it should be pointed out this is only an initial bifurcation shape since no cross-boundary tangential continuity can be guaranteed along with hole

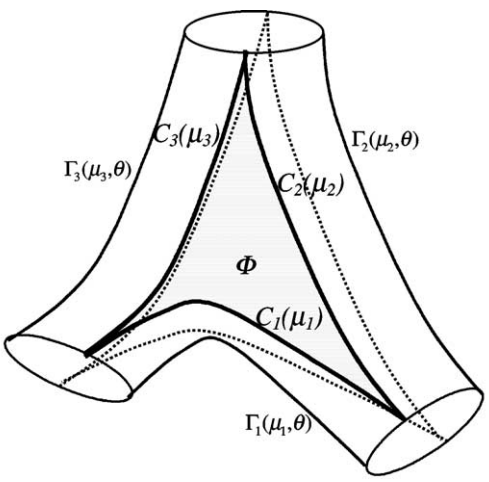

Fig. 5. Bifurcation surface sweeping.

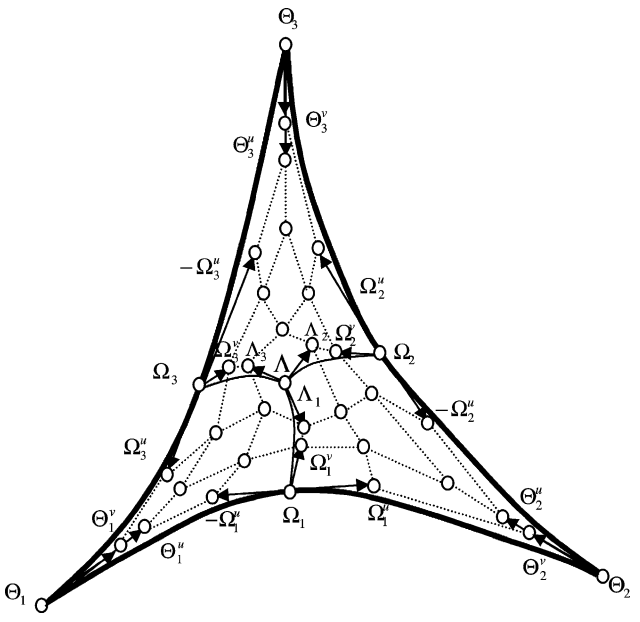

Fig. 6. Hole filling using Gregory–Zhou's approach.

boundaries. Therefore, we need to devise algorithms for modifying the initial shape to obtain GC^1 bifurcation.

4.6. GC^1 constructive modification of hole boundaries

The original boundary curves $C_i(\mu_i)$ are cubic Bézier with control polygon $\{P_{i,0}, P_{i,1}, P_{i,2}, P_{i,3}\}$. To achieve a smooth filling with tangential continuity, a modification for boundary curve $C_i(\mu_i)$ is required and can be performed as follows.

(i) Compute $C_i''(1) = 6(P_{i,2} - 2P_{i,1} + P_{i,0})$, $i = 1, 2, 3$;
(ii) Compute tangent vectors T_i and $T_{i,i}$, $(i = 1, 2, 3)$ of the curves.
(iii) Compute the normal N_i of plane Π_i spanned by $(T_i, T_{i,i})$.
(iv) Project $C_{i-1}''(1)$ onto plane Π_i : $\bar{C}_{i-1}''(1) = C_{i-1}''(1) - (C_{i-1}''(1)\cdot N_i)N_i$.
(v) Compute $\bar{C}_i''(0) = -\lambda_i^{-2}\bar{C}_{i-1}''(1) + \lambda_i^{-1}(\alpha_i p_{i-1}'(1) - p_i'(0))T_{i,i} - (q_{i-1}'(1) + \lambda_i^{-1}q_i'(0))T_i$.
(vi) Compute $\delta_{i0} = \bar{C}_i''(0) - C_i''(0)$ and $\delta_{i1} = \bar{C}_i''(1) - C_i''(1)$.
(vii) Degree-elevate $C_i(\mu_i)$ from cubic to degree 4.
(viii) Modify the two mid control points of the elevated curve to form a new control polygon as $\{P_{i,0}, (2P_{i,0} + 3P_{i,1})/5, (P_{i,0} + 6P_{i,1} + 3P_{i,2})/10 + \delta_{i0}/20, (3P_{i,1} + 6P_{i,2} + P_{i,3})/10 + \delta_{i1}/20, (3P_{i,2} + 2P_{i,3})/5, P_{i,3}\}$.

4.7. Modification for semi-tubular patches $\Gamma_i(\mu_i, \theta)$

After the boundary curves $C_i(\mu_i)$ are changed, the semi-tubular surfaces $\Gamma_i(\mu_i, \theta)$ $(i = 1, 2, 3)$ need to be degree-elevated to degree 5 along μ_i parameter direction accordingly. The change of the control points of curves $C_i(\mu_i)$ need to be reflected in the control points of $\Gamma_i(\mu_i, \theta)$ consistently.

To ensure the vector-valued cross-boundary derivatives of $\Gamma_i(\mu_i, \theta)$ along $C_i(\mu_i)$ to be cubic, the two middle control points of the row next to $C_i(\mu_i)$ need to be modified by the same amounts ($\delta_{i0}/20$ and $\delta_{i1}/20$, respectively) of the two middle control points of $C_i(\mu_i)$. This is because, the derivatives along the boundaries can be represented as a function of the subtraction of the corresponding control points of the two rows. If the displacements at the corresponding control points in the two rows are the same, the derivatives of the modified boundaries will remain unchanged in cubic form even though the boundaries of the hole are quintic.

4.8. Construction of hole boundary derivatives $D\Phi_i(\mu_i)$

With the modified hole boundaries and modified semi-tubular surfaces, the vector-valued cross-boundary derivative $D\Phi_i(\mu_i)$ can be determined with Eq. (3) and scalar functions $p_i(\mu_i)$ and $q_i(\mu_i)$. It can be converted as a quintic vector-valued Bézier function using the algorithm in Ref. [43].

Suppose

$$D\Gamma_i(\mu_i) = 3\sum_{j=0}^{3} D\Gamma_{ij}B_{j3}(\mu_i)$$

and

$$C_i'(\mu_i) = 5\sum_{j=0}^{4} DC_{ij}B_{j4}(\mu_i)$$

Then

$$D\Phi_i(\mu_i) = \sum_{j=0}^{5} D\Phi_{ij}B_{j5}(\mu_i)$$

can be determined as follows:

$$D\Phi_{i0} = 5\lambda_i\xi_i D\Gamma_{i0}$$

$$D\Phi_{i1} = (6\xi_i D\Gamma_{i0} + 20\lambda_i D\Gamma_{i1} - 5\lambda_{i+1}^{-1}DC_{i0})/5$$

$$D\Phi_{i2} = (18\xi_i D\Gamma_{i1} + 30\lambda_i D\Gamma_{i1} - 20\lambda_{i+1}^{-1}DC_{i1})/20$$

$$D\Phi_{i3} = (18\xi_i D\Gamma_{i2} + 20\lambda_i DC_{i3} - 30\lambda_{i+1}^{-1}DC_{i2})/20$$

$$D\Phi_{i4} = (6\xi_i D\Gamma_{i3} + 5\lambda_i DC_{i4} - 20\lambda_{i+1}^{-1}DC_{i3})/5$$

$$D\Phi_{i5} = -5\lambda_{i+1}^{-1}DC_{i4}$$

4.9. Modification for filling triangle

$C_i(\mu_i)$ and $D\Phi_i(\mu_i)$ are then split into two at $\mu_i = 1/2$. They are then re-scaled from parameter intervals [0,1/2] and [1/2,1] to normalized parameter interval [0,1]. Thus, we have $C_{i,0}(\mu_i)$, $C_{i,1}(\mu_i)$, $D\Phi_{i,0}(\mu_i)$ and $D\Phi_{i,1}(\mu_i)$. A cubic Bézier curve with control points $\{P_i, i = 0, 1, 2, 3\}$ can be represented by a quintic Bézier curve by degree-elevation as follows:

$$\begin{bmatrix} P_0 & \dfrac{2P_0 + 3P_1}{5} & \dfrac{P_0 + 6P_1 + 3P_2}{10} & \dfrac{3P_1 + 6P_2 + P_3}{10} \\ & & \dfrac{3P_2 + 2P_3}{5} & P_3 \end{bmatrix}$$

Let $\{Q_i, i = 0, 1, 2, 3, 4, 5\}$ be the control points of the quintic Bézier curve, the above degree-elevation can be expressed in the matrix form

$$\begin{bmatrix} Q_0 \\ Q_1 \\ Q_2 \\ Q_3 \\ Q_4 \\ Q_5 \end{bmatrix} = M \begin{bmatrix} P_0 \\ P_1 \\ P_2 \\ P_3 \end{bmatrix}$$

where

$$M = \begin{bmatrix} 1 & 0 & 0 & 0 \\ 0.4 & 0.6 & 0 & 0 \\ 0.1 & 0.6 & 0.3 & 0 \\ 0 & 0.3 & 0.6 & 0.1 \\ 0 & 0 & 0.6 & 0.4 \\ 0 & 0 & 0 & 1 \end{bmatrix}$$

For the surface case, we have the control net relation before and after the degree-elevation as follows:

$$\lfloor Q_{i,j} \rfloor_{6\times 6} = M \lfloor P_{i,j} \rfloor_{4\times 4} M^{\mathrm{T}}$$

To generate the final surface patches for hole filling, the star-lines and their associated vector-valued cross-boundary derivatives should be degree-elevated to quintic forms. Each of the filling patches has two star-line boundaries inside the filling triangle, and the other two boundaries being on the hole boundaries. The final filling surfaces can be generated based on the star-lines, split hole boundaries, and the vector-valued cross-boundary derivatives along the star-lines and the split hole boundaries. The entries for the control point matrix $\{Q_{i,j}, i,j = 0,1,2,3,4,5\}$ are as follows:

(i) The last (fifth) row and column of the control points are from the split hole boundaries.
(ii) The second to last (fourth) row and column of control points are from the sum of the control points of the split hole boundaries and 1/5 of the control vectors of the vector-valued cross-boundary derivatives along the split hole boundaries.
(iii) The first (0th) row and column of the control points in the matrix are from the star-lines.
(iv) The control points in the second (first) row and column in the matrix are from the sum/subtraction of the control points of the star-lines and 1/5 of the control vectors of the vector-valued cross-boundary derivatives along the star-lines.
(v) The remaining control points $\{Q_{i,j}, i,j = 2,3\}$ are yet to define.

Now, let us consider how to determine the undefined interior control points. A Bézier curve with control points $\{Q_i, i = 0,1,2,3,4,5\}$ becomes a cubic Bézier curve with control points $\{P_i, i = 0,1,2,3\}$ if and only if:

$$P_0 = Q_0; \qquad P_3 = Q_5$$

$$3(P_1 - P_0) = 5(Q_1 - Q_0)$$

$$3(P_3 - P_2) = 5(Q_5 - Q_4)$$

Thus

$$P_1 = (5Q_1 - 2Q_0)/3; \qquad P_2 = (5Q_4 - 2Q_5)/3$$

we have

$$Q_2 = \frac{P_0 + 6P_1 + 3P_2}{10} = \frac{-3Q_0 + 10Q_1 + 5Q_4 - 2Q_5}{10}$$

$$Q_3 = \frac{3P_1 + 6P_2 + P_3}{10} = \frac{-2Q_0 + 5Q_1 + 10Q_4 - 3Q_5}{10}$$

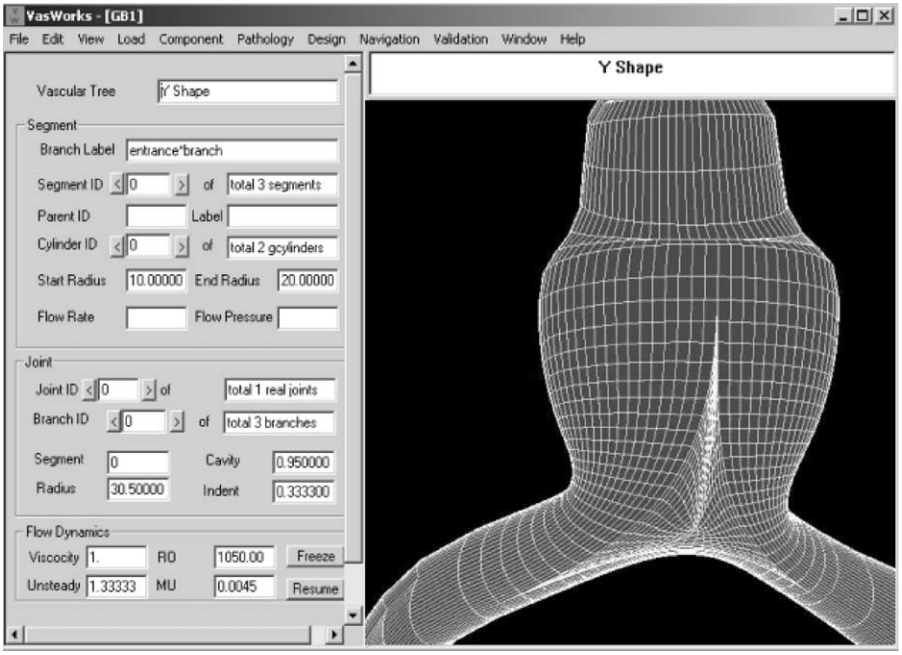

Fig. 7. User Interface design with the VasWorks.

or in matrix form

$$Q_i = N_i \begin{bmatrix} Q_0 \\ Q_1 \\ Q_4 \\ Q5 \end{bmatrix}, \qquad i = 2,3$$

where

$$\begin{bmatrix} N_2 \\ N_3 \end{bmatrix} = \begin{bmatrix} -0.3 & 1.0 & 0.5 & -0.2 \\ -0.2 & 0.5 & 1.0 & -0.3 \end{bmatrix}$$

Using the Coons–Boolean sum approach for surface construction and the algorithm described in Ref. [43], the remaining interior control points $\{Q_{i,j}, i,j = 2,3\}$ can be determined as follows:

$$Q_{i,j} = N_i \begin{bmatrix} Q_{i0} \\ Q_{i1} \\ Q_{i4} \\ Q_{i5} \end{bmatrix} + N_j \begin{bmatrix} Q_{0j} \\ Q_{1j} \\ Q_{4j} \\ Q_{5j} \end{bmatrix} - N_i \begin{bmatrix} Q_{00} & Q_{01} & Q_{04} & Q_{05} \\ Q_{10} & Q_{11} & Q_{14} & Q_{15} \\ Q_{40} & Q_{41} & Q_{44} & Q_{45} \\ Q_{50} & Q_{51} & Q_{54} & Q_{55} \end{bmatrix} N_j^{\mathrm{T}}$$

Finally, we have three new bi-quintic Bézier patches Φ_i. The three new Bézier patches Φ_i $(i = 1,2,3)$ are not only tangent to each other along the star-lines, but also tangent to the surrounding surfaces along their common boundaries. The triangular hole can then be filled with the union of the three new surface patches Φ_i, $(i = 1,2,3)$.

5. Applications

We have described the constructive algorithms for 3D vascular reconstruction. In this section, we demonstrate some of selected applications of the algorithms. The algorithms have been incorporated in our vascular modeling system called VasWorks. A User Interface (UI) with the VasWorks is designed using Visual C++ programming with Window PC platform (Fig. 7). Presently, the UI includes an object identity (text) panel, a graphics display panel, a control panel for modeling of vascular segment and bifurcation. The several visualization modes (such as line, meshed and shaded, etc.) are implemented with VasWorks.

The algorithms developed are able to model various bifurcation shapes (such as Y-shapes, T-shapes or arrow-like shapes, etc.) with good flexibility. The bifurcation can be either planar or non-planar. The sizes of the individual branches can vary from one to another. Fig. 8(a) shows a smooth vascular segment modeled and Fig. 8(b) shows a bifurcation modeled with the proposed constructive algorithms. We use the algorithms developed to visualize various diseased lesions. Fig. 9 shows an example of a carotid artery bifurcation modeled with the proposed method. Fig. 10 shows another example of the cerebral vasculature reconstructed from the vascular volume images. In Fig. 10(a), a cerebral aneurysm is clearly visualized and Fig. 10(b) shows the volume rendered head with superimposed vascular networks using a selective cropping to reveal the cerebral arteries.

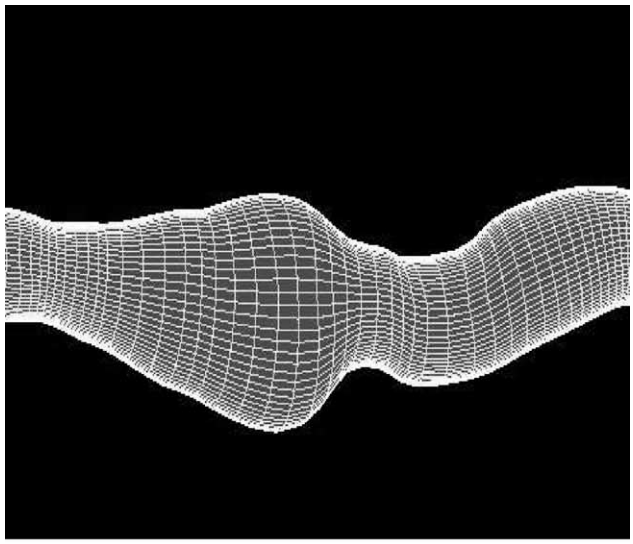

(a) Vascular segments

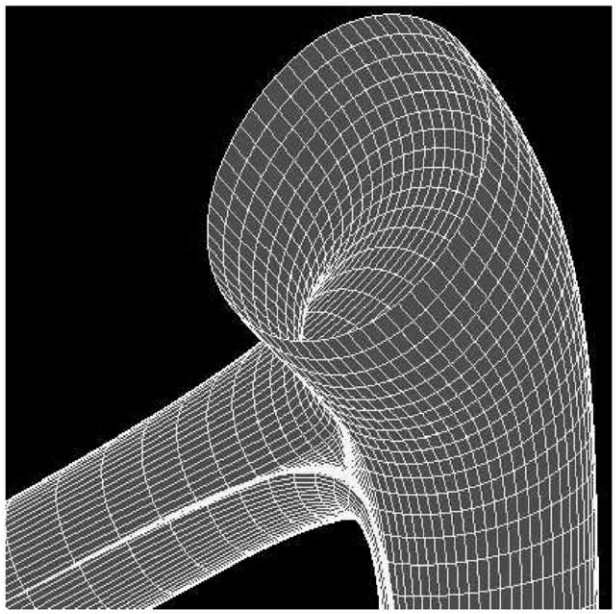

(b) Vascular bifurcation

Fig. 8. Vascular modeling for both segment and bifurcation.

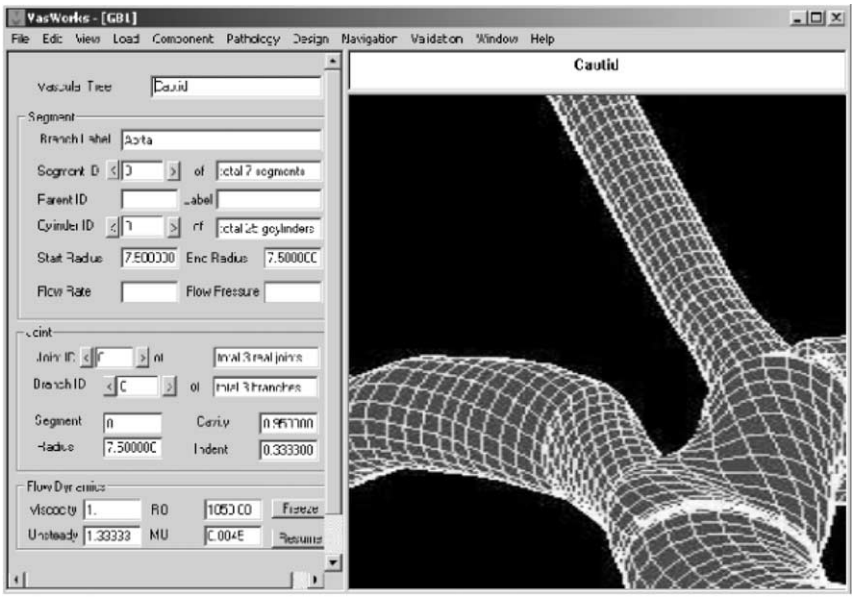

Fig. 9. Stenosis modeling at a carotid bifurcation.

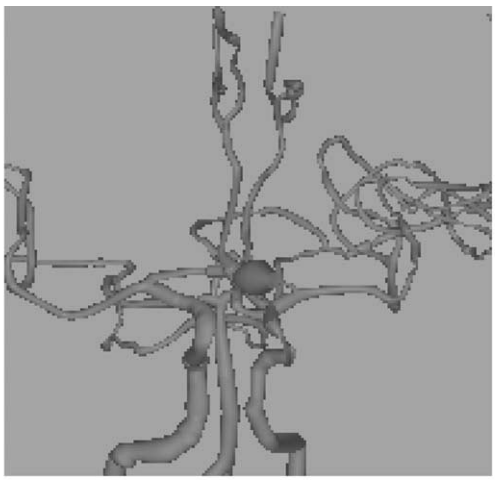

(a) Human vascular cerebral arteries

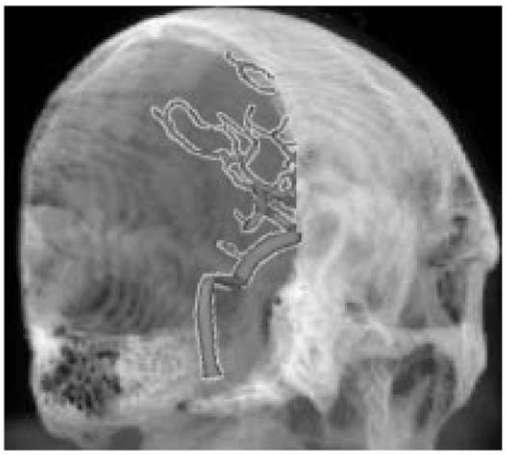

(b) Selectively cropped cerebral arteries superimposed on volume rendered brain

Fig. 10. Modelling cerebral arteries on the volume rendered human head.

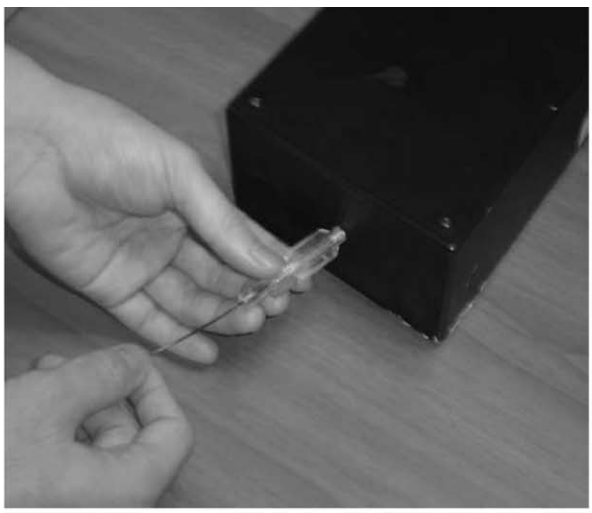

(a) A haptic device for Manipulating of catheters and guidewires

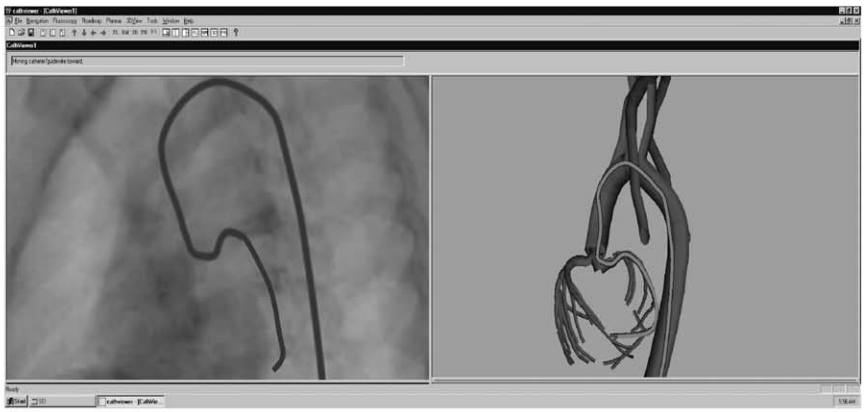

(b) Navigating of the catheters and guidewires (left view) under fluoroscopic guidance within the vascular networks (right view)

Fig. 11. Simulation of vascular catheterization.

With the reconstructed 3D surface models of vasculature, simulation of the catheterization and other related minimally invasive surgical procedures can be performed. We have developed a haptic device (Fig. 11(a)) to allow users manipulating on real catheters and guidewires. Fluoroscopic imaging (Fig. 11(b)) is also developed and integrated with the simulation system for the training of hand–eye coordination in image-guided catheterization procedures.

6. Conclusions

This paper presents constructive algorithms to model vascular networks. Sweeping and blending operations are used to create initial vascular segments and bifurcations. In particular, piecewise Bézier patches are generated to represent the vascular segments. As for the bifurcation, three semi-tubular bi-cubic Bézier patches are generated using sweeping operation. Two three-sided holes are formed surrounded by three semi-tubular patches. Each hole is filled with three bi-cubic Bézier patches. Constructive methods for modifying vascular joints are developed to form GC^1 vascular networks. First, the boundaries and the row next to the boundaries of semi-tubular patches are modified to quintic form to allow cross-boundary tangential continuity, twist compatibility and unique existence of tangential plane. The new boundaries and derivatives of the holes are used to generate new filling triangles.

Bifurcation of blood vessels is an interesting growing process of the vascular anatomy development. The current vascular modeling assumes no multiple branching with the vascular network. When encountering multi-branching structures, we can separate them into several bifurcations. However, this may cause

difficulty when two separated bifurcations are very close to each other. The present algorithms are based on the blending ideas for the modeling of vascular networks. Sweeping and hole filling is applied for the bifurcation where the hole is three-sided. The concept can be applied to multi-sided hole filling for generating multi-branching vessels.

Acknowledgements

This research was sponsored by the Singapore's Agency of Science, Technology, and Research (A*STAR). The second author would like to thank Zhejiang University for the support of his Chang Kong professorship.

References

[1] Chen SJ, Carroll JD. 3-D reconstruction of coronary arterial tree to optimize angiographic visualization. IEEE Trans Med Imaging 2000; 19(4):318–36.
[2] Schreiner W, Buxbaum PF. Computer-optimization of vascular trees. IEEE Trans Biomed Engng 1993;40(5):482–91.
[3] Sequeira J, Ebel R, Schmitt F. Three-dimensional modeling of tree-like anatomical structures. Comput Med Imaging Graph 1993;17(4/5): 333–7.
[4] Hademenos GJ. The physics of cerebral aneurysms. Physics Today 1995;Feb:24–30.
[5] Pao YC, Liu JT, Ritman EL. Bending and twisting of an in vivo coronary artery at a bifurcation. J Bio-mech 1992;25:287–95.
[6] Nichols WW, O'Rourke MF. McDonald's series: blood flow in arteries. UK: Oxford University Press; 1997.
[7] Wang Y, Chui C, Lim H, Cai Y, Mak K. Real-time interactive simulator for percutaneous coronary revascularization procedures. Comput Aided Surg 1999;3(5).
[8] Cai Y, Wang Y, Ye X, Chui C, Ooi Y, Mak K. Catheter design, validation and presentation using CathWorks. Int J Robotics Automat 2000;15(1):27–33.
[9] Nakajima S, Atsumi H, Bhalerao A, Jolesz F, Kikinis R, Yoshimine T, Moriarty T, Stieg P. Computer-assisted surgical planning for cerebrovascular neurosurgery. Neurosugery 1997;38: 403–9.
[10] Saito T, Misaki M, Shirato K, Takishima T. Three-dimensional quantitative coronary angiography. IEEE Trans Biomed Engng 1990; 37(8):768–77.
[11] Beier J, Siekmann R, Müller F, Tröger J, Schedel H, Biamino G, Fleck E, Felix R. Planning and control of artic stent implantations using 3D reconstructions based on computer tomography. In: Lemke HU, Vannier MW, Inamura K, editors. Computer assisted radiology. The Netherlands: Elsevier; 1996. p. 716–20.
[12] Rubin GD. Computed tomographic angiography before and after aortic stent-grafting. J Vasc Intervent Radiol 1999;10(2 Part 2): 88–92.
[13] Rubin GD, Paik DS, Johnston PC, Napel S. Measurements of the aorta and its branches with helical CT. Radiology 1998;206(3): 823–9.
[14] Broeders IAJM, Blanensteijn JD, Olree M, Mali WPThM, Eikelboom BC. Preoperative sizing of grafts for transfemoral endovascular aneurysm management: a prospective comparative study of spiral CT angiography, arteriography, and conventional CT imaging. J Endovasc Surg 1997;4:252–61.
[15] Lorensen WE, Cline HE. Marching cubes: a high resolution 3-D surface construction algorithm. Comput Graph (SIGGRAPH'87) 1987;21(4):163–9.
[16] Garland M, Heckbert P. Surface simplification using quadric error bounds. Proc ACM SIGGRAPH97 1997;209–16.
[17] Xia J, El-Sana J, Varshney A. Adaptive real-time level-of-detail-based rendering for polygonal models. IEEE Trans Vis Comput Graph 1997;3:171–83.
[18] Kaufman A. Volume rendering. Las Alamitos, CA: IEEE Computer Science Press; 1990.
[19] Ehricke HH, Donner K, Koller W, Strasser W. Visualization of vasculature from volume data. Comput Graph 1994;18(3): 395–406.
[20] Cline HE, Lorensen WE, Herfkens RJ, Johnson GA, Glover GH. Vascular morphology by three-dimensional magnetic resonance imaging. Magn Reson Imaging 1989;7:45–54.
[21] Puig A, Tost D, Navazo I. An interactive cerebral blood vessel exploration system. Proc Vis'97 1997;443–6.
[22] Solzbach U, Oser U, Rombach MR, Wollschlager H, Just H. Optimum angiographic visualization of coronary segments using computer-aided 3D-reconstruction from biplane views. Comput Biomed Res 1994;27(3):178–98.
[23] Nguyen TV, Sklansky J. Reconstructing the 3-D medial axes of coronary arteries in single-view cine-angiogrames. IEEE Trans Med Imaging 1994;13(3):61–73.
[24] Longuet-Higgins HC. A computer algorithm for reconstructing a scene from two projections. Nature 1981;293(10):133–5.
[25] Faugeras OD. Three-dimensional computer vision: a geometrical viewpoint. Cambridge, MA: MIT Press; 1993.
[26] Garreau M, Coatrieux JL, Collorec R, Chardenon C. A knowledge-based approach for 3D reconstruction and labeling of vascular networks from biplane angiographic projections. IEEE Trans Med Imaging 1991;10(2):122–31.
[27] Smets C, Vandewerf F, Suetens P, Oosterlinck A. An expert system for the labelling and 3-D reconstruction of the coronary arteries from two projections. Int J Card Imaging 1990;5(2/3): 145–54.
[28] Kass M, Witkin A, Terzopoulos D. Snakes: active contour models. Int J Comput Vis 1987;1:321–31.
[29] Lee TC, Kashyap RL, Chu CN. Building skeleton models via 3D medial surface/axis thinning algorithms. CVGIP: Graph Models Image Process 1994;56(6):462–78.
[30] Arcelli C, Sanniti di Baja G. Euclidean skeleton via centre-of-maximal-disc extraction. Image Vis Comput 1993;11(2): 163–73.
[31] Pellot C, Herment A, Sigelle M, Horain P, Maitre H, Peronneau P. A 3-D reconstruction of vasculature structures from two X-ray angiograms using an adapted simulated annealing algorithm. IEEE Trans Med Imaging 1994;13(1):48–60.
[32] Brandt JW, Algazi VR. Continuous skeleton computation by Voronoi diagrams. CVGIP: Image Understand 1992;55(3):329–37.
[33] Brown AD, Wheal HV, Stockley EW. The reconstruction of neurone morphology from thin optical sections: graphical aspects. Proc EUROGRAPH'87 1987;113–24.
[34] Barillot C, Bibaud B, Scarabin J-M, Coatrieux J-L. 3D reconstruction of cerebral blood vessels. IEEE Trans Comput Graph Appl 1985;Dec: 13–19.
[35] Van Leeuwen GMJ, Kotte ANTJ, Lagendijk JW. A flexible algorithm for construction of 3-D vessel networks for use in thermal modeling. IEEE Trans Biomed Engng 1998;45(5):596–604.
[36] Ferley E, Cani-Gascuel M-P, Attali D. Skeletal reconstruction of branching shapes. Comput Graph Forum 1997;16(5):283–93.
[37] Farin GE. Curves and surfaces for computer aided geometric design. Boston: Academic Press; 1988.
[38] Piegl L, Tiller W. The NURBS book. Berlin: Springer; 1995.

[39] Ye X, Nowacki H, Patrikalakis NM. GC^1 multisided Bézier surface. Engng Comput 1997;13:222–34.
[40] Goldapp M. Approximation of circular arcs by cubic polynomial. Comput Aided Geom Des 1991;8:227–38.
[41] Maekawa T, Patrikalakis NM, Sakkalis T, Yu G. Analysis and applications of pipe surfaces. Comput Aided Geom Des 1998;15:437–58.
[42] Gregory JA, Zhou JW. Filling polygonal holes with bicubic patches. Comput Aided Geom Des 1994;11:391–410.
[43] Ye X. Generating Bézier points for curves and surfaces from boundary information. Comput Aided Des 1995;27:875–85.
[44] Sederberg T, Hong M, Kaneda K, Klimaszewski K. Triangulation of branching contours using area minimization. Int J Comput Geom Appl 1998;8(4):389–406.
[45] Choi Y-K, Park KH. A heuristic triangulation algorithm for multiple planar contours using an extended double branching procedure. Vis Comput 1994;10:372–87.